Hindawi
Mathematical Problems in Engineering
Volume 2021, Article ID 9948745, 12 pages
https://doi.org/10.1155/2021/9948745

Research Article

Mathematical Analysis of the 08 May 2014 Weak Storm

Kevser Köklü

Yildiz Technical University, Department of Mathematical Engineering, Davutpasa Campus, İstanbul 34220, Turkey

Correspondence should be addressed to Kevser Köklü; kevserkoklu@gmail.com

Received 13 March 2021; Accepted 14 August 2021; Published 16 September 2021

Academic Editor: Taseer Muhammad

Since the time scale of weak storms is about half the time scale of intense storms, it is troublesome and important to examine the solar wind parameters/interplanetary magnetic field (IMF) (E, v, P, T, N, and B_z) to evolve and affect to zonal geomagnetic indices (Kp, Dst, AE, and ap). In a severe storm, which usually has two main phases, solar parameters have enough time to react, but weak storms cannot find this time. They have to yield their reaction in a short time. One can find a weak storm in order to reveal and discuss the consistency of models that have proven themselves in severe and moderate storms in this study. I discuss weak storm (Dst = −46) on May 8, 2014, via solar wind parameters and zonal geomagnetic indices. The goal of the work is to realize the models applicable to the moderate and the strong storms for a weak storm. Hereby, all possible correlations between solar parameters and zonal indices are discussed in depth. I tried to obey the cause-effect relationship while creating mathematical models while not ignoring the physical principles. Therefore, the physical principles govern the study. The results are visualized with tables and graphs for the understanding of the dynamic structure of the storm.

1. Introduction

A geomagnetic storm [1–23] is a characteristic event of nature that continues for 1–3 days and covers all the magnetosphere from the Earth's surface to the magnetotail. If the variables that cause such recurring phenomena are well analyzed, the event processor can be understood easily. Good analyses can also lead to meaningful discussion in other phenomena. In a geomagnetic storm, the cause-effect relation and the causality principle [15–18, 24–26] are physically restrictive. The solar wind plasma parameters of the phenomenon: electric field (E), flow velocity (v), solar wind dynamic pressure (P), temperature (T), proton density (N), and magnetic field (B_z), are the "causes." Kp, ap, Dst, and AE, the zonal geomagnetic indices of the storm, are the "effects" [27–32]. Dst (disturbance storm time) is a geomagnetic index that confirms the magnitude of the geomagnetic storms that cover the Earth. It is the average of the horizontal component of the geomagnetic field obtained from stations in different geographical regions of the world. Kp (planetary index) is obtained by a weighted average of kind exes in 13 subauroral observations. A linear index is obtained from ap and Kp. The AE index is a snapshot general index as a measure of changes in global Auroral Electrojet activity as defined by Davis and Sugiura [33].

Solar wind parameters and zonal geomagnetic indices are the main elements of the dynamic structure of the storm. This plasma-dense dynamic medium has energy-charged particles that flow out at high speed from the Sun [27]. Such an intense dynamic structure causes rapid changes in the magnetic field of the Sun's plasma-intensive environment. The coronal mass ejection (CME) cloud swallows the Earth's magnetosphere. Meanwhile, B_z component of B magnetic field of CME cloud is negatively charged to the southward. Geomagnetic disturbances occur with the magnetic reconnection [32, 34, 35], between this component and the Earth's magnetic field. The CME causes direct solar wind parameters to change, and then the storm process begins [36, 37].

In order to discuss the dynamic structure of the storm, it is necessary to establish models by looking at the relationships between the variables and to keep the consistency of these correlations. The mathematical models can guide researchers about data and their relationships whichever in the science area [15, 20]. In addition, they may yield clues about the behavior of the variables under different terms [15, 16, 18, 26, 38, 39].

In this study, the models established with the deterministic and pragmatic approach of Eroglu [15] for geomagnetic storms are discussed for a weak phenomenon for the first time. 8 May 2014 weak storm is analyzed with this mathematical perspective. Models [15, 16] have had a new identity with the 08 May 2014 geomagnetic storm [40]. The formulated models are exactly dependent on the stochastic processes [41]. Visualized models give the readers opportunities to compare correlation data. Although binary linear models may find it difficult to explain the exact relationship between variables, the presentation of these models is necessary [15, 16]. In the paper, it reveals, with obeying to the physical perspective, that the variables of solar wind parameters and zonal geomagnetic indices do not interact randomly, although they exhibit normal distribution. Weak correlation encourages scientists to seek nonlinear models.

Section 2 presents the Sun parameters, regional geomagnetic indexes, and the five-day distributions of variables. In Section 3 the analyses are performed. Section 4 provides a discussion.

2. Data

In this study, Space Physics Environmental Data Analysis Software (SPEDAS) is used. Analysis Software data are IDL-based. It is reachable at this link: https://themis.igpp.ucla.edu/software.shtml.

Hourly OMNI-2 Solar Wind and IMF parameter data can be accessed online. In addition, Dst and AE indices were obtained from the World Geomagnetism Data Center Kyoto using SPEDAS. From the NGDC by using SPEDAS with CDA Web Data Chooser (space physics public data), Kp and ap are obtained. For 2014 May weak storm, solar wind dynamic pressure, IMF, electric field, flow speed, and proton density were recorded in the OMNI hourly data. Geomagnetic classification [42] is shown in Table 1.

The characteristic of the phenomenon at the weak level (Dst = −46 nT) on 08 May 2014 have been investigated. Figure 1 demonstrates the OMNI data set from 00:00 UT on 06 May 2014 to 00:00 UT on 10 May 2014. The plot interval includes the storm day (2014 May 08), two days before and two days after the storm (120 hours). The May storm started on May 08th with CME at 06:00 UT. The gradually decreasing magnetic field component (B_z) reaches the negative peak value −9.2 nT at 07:00 UT. Meanwhile, as the plasma flow speed (v) catches 329 km/s, its maximum value, the electric field (E) reaches 3.03 mV/m its maximum value and the geomagnetic aurora electrojet index (AE) raises to its maximum value of 767 nT. Finally, Dst hits its peak value of −46 nT at 08:00 UT.

Figure 1 can be shortly detailed as follows: On 06.05.2014 at 07:00 UT when B_z component is at its minimum (−9.2 nT), Dst index dwindled to −39 nT, and the electric field E attains its maximum value of 3.03 mV/m. Meantime, plasma flow speed v minimum value becomes 329 km/s, and AE index catches its peak value 767 nT. Within a few hours, Dst index indicates its minimum value −46 nT, ap index hits its maximum value 39 nT, and proton density N reaches its peak value 21.51/cm^3.

On 09.05.2014 at 11:00 UT when B_z component is maximum (6 nT), the electric field E catches −2.25 mV/m, proton density N takes 6.31/cm^3, AE index diminishes to 69 nT, and ap index decreases to 4 nT. As this comes to cross Dst index reaches −10 nT.

3. Mathematical Modeling

The expressive analysis valuation of the geomagnetic storm in May 2014 is shown in Table 2. Specifically, the peak and deviation values give the reader information about the data range. The more the increase in the standard deviation of a variable, the more it become distant to average. This weakens the effect of the variable. When Table 2 is taken into account, the most stable variables are E, P, B_z, ap, N, and Dst, respectively. Physically, ap and Dst zonal geomagnetic indices are a result of P, E, B_z, and N solar wind parameters by reason of cause-effect principle. In Table 3, binary instantaneous correlations of the data are given. Correlation analysis is an auxiliary regression analysis method. As the table values approach ±1, the bond between the variables is stronger. The high relation level in Table 3 plays an important role in modeling [15, 16].

KMO and Bartlett's test table in Table 4 gives an idea of the data for factor analysis. It can be mentioned that the variables are normally distributed if the value obtained by measuring the Kaiser–Meyer–Olkin sampling capability is close to 1.0. As can be seen from Table 4, the variable set of this storm is suitable for factor analysis.

Variables cluster is displayed in Figure 2(a) hierarchically. Figure 2(b) displays scattering of variables. The varimax method indicates sprinkling of the variables along two main axes. E, AE, ap, Kp N, and P lie on one side, and Dst, B_z, v, and T lie on the other side in Figure 2(b). If one pays attention, E and B_z are split symmetrically into two opposing sides in Figure 2(b).

In the factor analysis with no composite variables, each variable is handled separately. Variables are examined more specifically (with the principal component) by the principal component analysis. In Table 5, the maximum two eigenvalues of the covariance matrix constitute 78% of the total change when changed in the ten-variable data reduction method. This means that in Table 5, 78% of the phenomenon can be explained by modeling with the variables at hand.

Scattering plot of these variables is presented in Figure 3. It is ranked from the maximum between the variables, with the showing a factor between every two points.

For the rotation matrix, varimax examines the linear grouping of event variables by the Kaiser normalization method. The method that approaches each variable as a factor indicates the contribution and weight of these factors to linear clustering. Table 6 is the table of these weights.

Table 1: Geomagnetic storm Dst index.

Class	Number	%	Dst range (nT)
Weak	482	44	−30 to −50
Moderate	346	32	−50 to −100
Strong (i.e., intense)	206	19	−100 to −200
Severe (very intense)	45	4	−200 to −350
Great	6	1	<−350

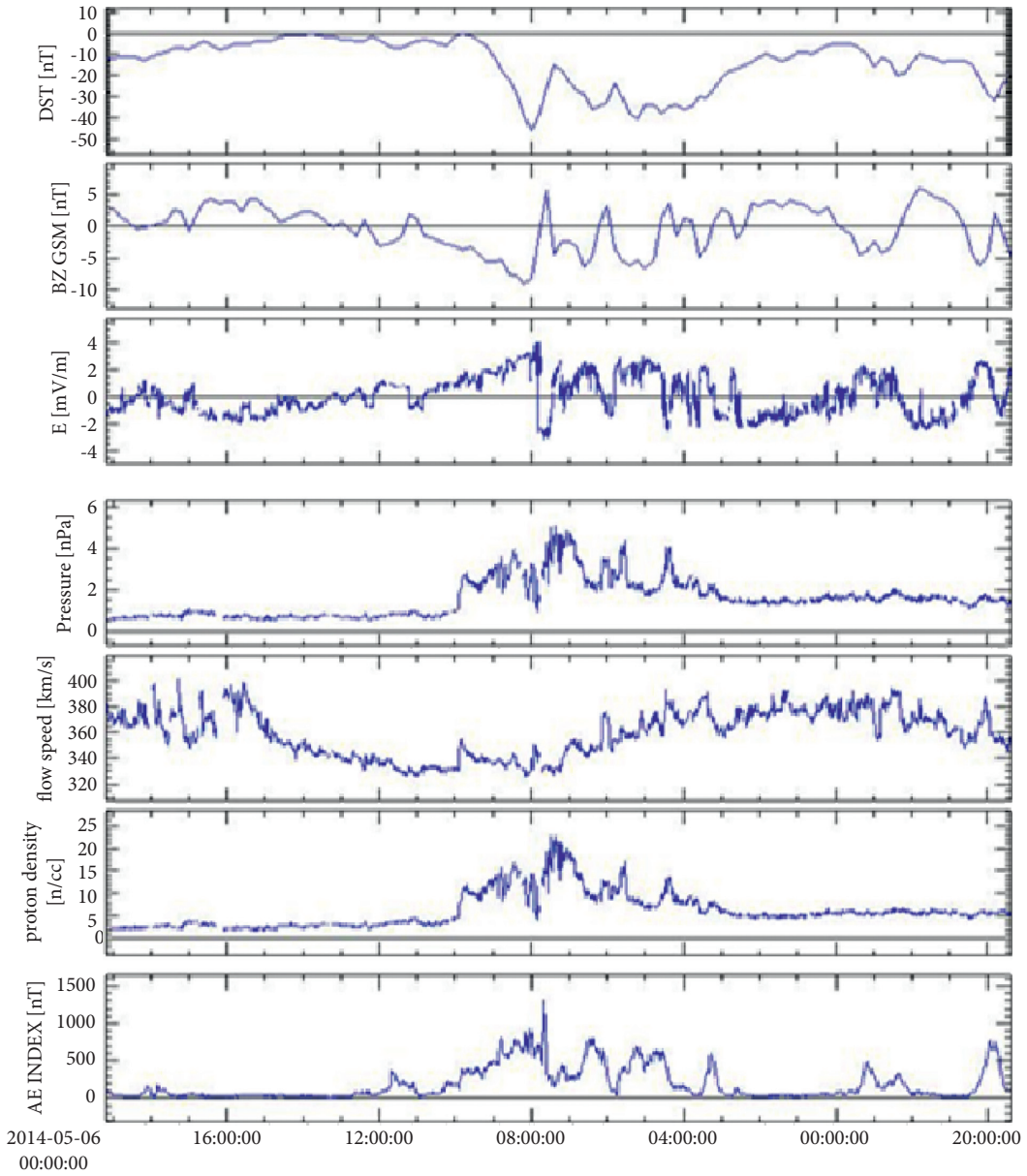

Figure 1: From top of the bottom parameters shown in Dst index, electric field E (mV/m), magnetic field B_z (nT), flow speed v (km/s), proton density N (1/cm^3), solar wind dynamic pressure P (nPa), and aurora electrojet AE (nT) index for 2014 May 06–10 (from NASA NSSDC OMNI data set).

Table 2: Descriptive analysis.

	N	Minimum	Maximum	Mean	Std. deviation
B_z (nT)	120	−9.2	6.0	−0.328	3.5401
T (K)	120	10235	150108	59373.94	31491.411
N (1/cm^3)	120	1.9	21.5	6.365	4.1058
v (km/s)	120	329	390	359.25	17.974
P (nPa)	120	0.5	4.5	1.513	0.9131
E (m V/m)	120	−2.3	3.0	0.091	1.2649
Kp	120	1	47	15.08	13.082
Dst (nT)	120	−46	0	−14.33	11.538
ap (nT)	120	1	39	7.78	8.264
AE (nT)	120	17	767	189.89	207.013

Table 3: Pearson's correlation matrix for the storm variables.

	B_z (nT)	T (K)	N (1/cm^3)	v (km/s)	P (nPa)	E (mV/m)	Kp	Dst (nT)	ap (nT)	AE (nT)
B_z (nT)	1	0.225*	−0.457**	0.426**	−0.428**	−0.999**	−0.652**	0.381**	−0.541**	−0.745**
T (K)		1	0.080	0.522**	0.190*	−0.212*	0.128	−0.521**	0.092	−0.057
N (1/cm^3)			1	−0.258**	0.984**	0.452**	0.768**	−0.566**	0.723**	0.638**
v (km/s)				1	−0.126	−0.418**	−0.223*	−0.026	−0.245**	−0.312**
P (nPa)					1	0.425**	0.771**	−0.612**	0.707**	0.617**
E (m V/m)						1	0.654**	−0.381**	0.543**	0.738**
Kp							1	−0.744**	0.944**	0.824**
Dst (nT)								1	−0.700**	−0.674**
ap (nT)									1	0.776**
AE (nT)										1

*and **correlation are significant at the 0.05 level (2-tailed) and at the 0.01 level (2-tailed), respectively.

Table 4: KMO and Bartlett's test.

Kaiser–Meyer–Olkin measure of sampling adequacy		0.731
Bartlett's test of sphericity	Approx. chi-square	2144.413
	Df	45
	Sig.	0.000

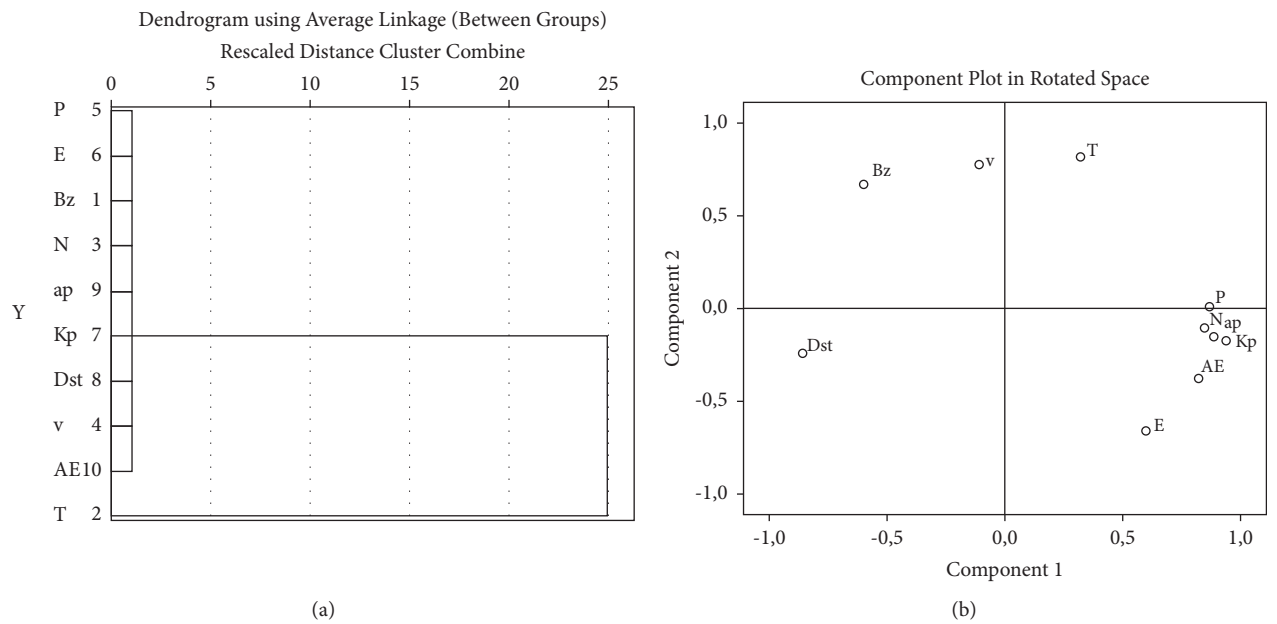

Figure 2: (a). Dendrogram of hierarchical cluster analysis. (b) Factor loadings for solution.

Table 5: Total variance explained.

Component	Initial eigenvalues			Extraction sums of squared loadings		
	Total	% of variance	Cumulative (%)	Total	% of variance	Cumulative (%)
1	5.751	57.5 15	57.515	5.751	57.515	57.515
2	2.050	20.4 98	78.013	2.050	20.498	78.013

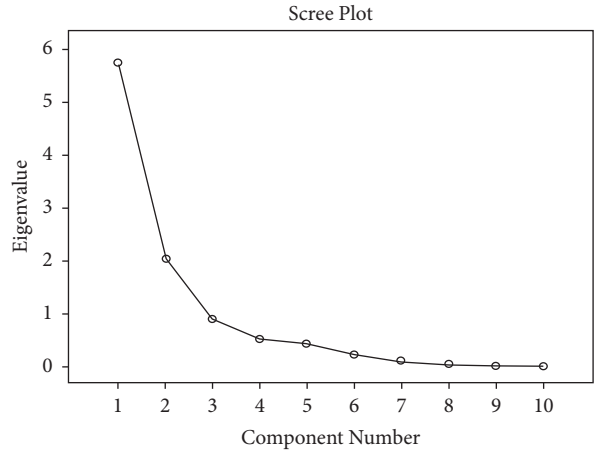

Figure 3: Scattering for eigenvalues.

Table 6: Rotated component matrix.

Component	B_z (nT)	T (K)	N (1/cm^3)	v (km/s)	P (nPa)	E (mV/m)	Kp	Dst (nT)	ap (nT)	AE (nT)
1	−0.599	0.322	0.846	−0.109	0.869	0.600	0.941	−0.859	0.886	0.823
2	0.667	0.816	−0.104	0.774	0.012	−0.659	−0.175	−0.241	−0.153	−0.375

Hence, these models can be written as follows with factor weights from Table 6:

$$\begin{aligned}\text{Axes 1} &= -(0.599)B_z + (0.322)T + (0.846)N - (0.109)v + (0.869)P + (0.600)E \\ &\quad + (0.941)\text{Kp} - (0.859)\text{Dst} + (0.886)\text{ap} + (0.823)\text{AE}, \\ \text{Axes 2} &= (0.667)B_z + (0.816)T - (0.104)N + (0.774)v + (0.012)P - (0.659)E \\ &\quad - (0.175)\text{Kp} - (0.241)\text{Dst} - (0.153)\text{ap} - (0.375)\text{AE}.\end{aligned} \tag{1}$$

Trying to catch an overview with the general linear models will aid to better understand the storm form. Binary views with some zonal geomagnetic indices (Dst, ap, and AE) and some solar wind parameters (magnetic field component (B_z), the electric field (E), temperature (T), flow velocity (v), proton density (N), and flow pressure (P)) can be seen in Figures 4–6, respectively. Figures 4–6 help for visualizing correlation of variables.

The analysis of variance of Dst index is shown in Table 7. It can be seen that regression coefficients are significant. This table shows how much of the residuals are explained by the variables in the linear regression model. Table 8 shows the model of the Dst index.

Binary views with Dst and B_z, T, P can be seen in Figure 4.

Table 9 shows that the model is significant, while Table 10 indicates the ap index.

Binary views with ap and N, E can be seen in Figure 5.

Table 11 indicates that the model is significant, while Table 12 shows the AE index.

Binary views with AE and B_z, N can be seen in Figure 6.

For many years, B_z-Dst linear relationship has been an important part of the researchers' discussions [43]. In addition to these discussions, the author tries to add depth to the meaning of the relationship between nonlinear models Dst, ap, and AE with B_z in addition to linear models. It can

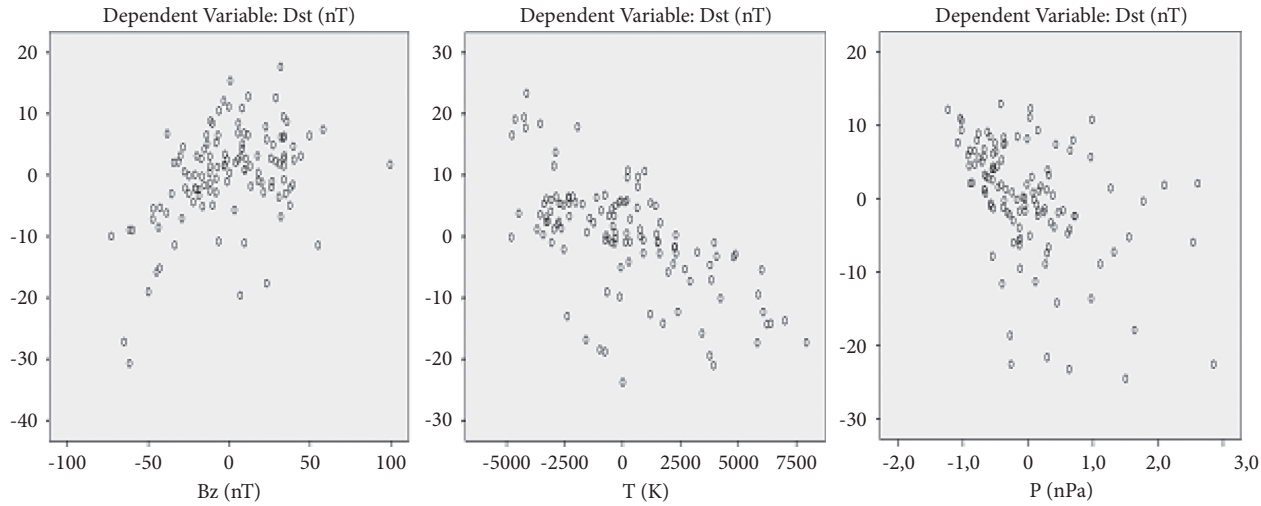

Figure 4: Binary views of Dst and B_z, T, P.

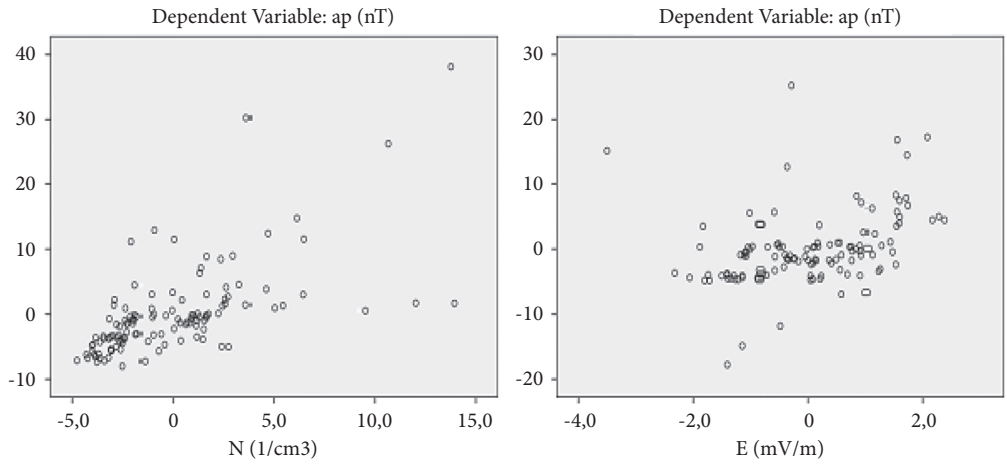

Figure 5: Binary views of ap and N, E.

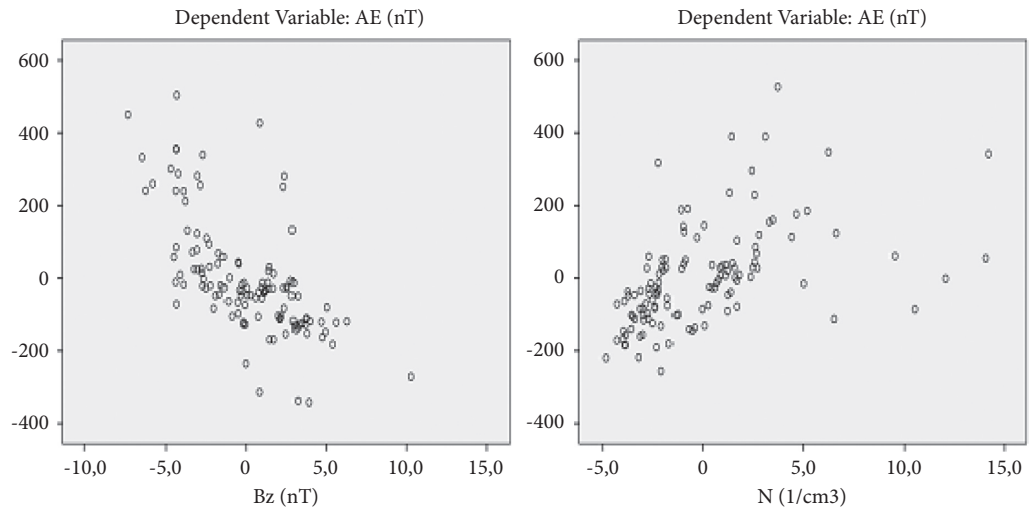

Figure 6: Binary views of AE and B_z, N.

Table 7: Anova (analysis of variance) of Dst. Dst = $(4.501) - (4.597)v + (0.001)T + (1.123)B_z$, where multiple determination coefficients R are 0.793.

Model	Sum of squares	df	Mean square	F	Sig.
Regression	9970.000	3	3323.333	65.667	0.000
Residual	5870.667	116	50.609		
Total	15840.667	119			

Table 8: Regression coefficients of Dst. Dst = $(4.501) - (4.597)v + (0.001)T + (1.123)B_z$, where multiple determination coefficients R are 0.793.

Model	Unstandardized coefficients	Standardized coefficients		t	Sig.	95% confidence interval for B	
	B	Std. error	Beta			Lower bound	Upper bound
Constant	4.501	1.639		2.747	0.007	1.256	7.747
P (nPa)	−4.597	0.835	−0.364	−5.503	0.000	−6.252	−2.943
T (K)	0.001	0.000	−0.529	−8.629	0.000	0.000	0.000
B_z (nT)	1.123	0.217	0.345	5.171	0.000	0.693	1.553

Table 9: Anova (analysis of variance) of ap. ap = $-(0.070) + (1.207)N + (1.779)E$, where multiple determination coefficients R are 0.762.

Model	Sum of squares	df	Mean square	F	Sig.
Regression	4725.017	2	2362.509	81.253	0.000
Residual	3401.908	117	29.076		
Total	8126.925	119			

Table 10: Regression coefficients of ap. ap = $-(0.070) + (1.207)N + (1.779)E$, where multiple determination coefficients R are 0.762.

Model	Unstandardized coefficients	Standardized coefficients		t	Sig.	95% confidence interval for B	
	B	Std. error	Beta			Lower bound	Upper bound
Constant	−0.070	0.975		−0.072	0.943	−2.001	1.861
N (1/cm^3)	1.207	0.135	0.600	8.944	0.000	−0.940	1.474
E (mV/m)	1.779	0.438	0.272	4.061	0.000	0.911	2.646

Table 11: Anova (analysis of variance) of AE index. AE = $(58.028) - (33.471)B_z + (18.990)N$, where multiple determination coefficients R are 0.816.

Model	Sum of squares	df	Mean square	F	Sig.
Regression	3399775.034	2	1699887.517	116.999	0.000
Residual	1699904.558	117	14529.099		
Total	5099679.592	119			

Table 12: Regression coefficients of AE index. AE = $(58.028) - (33.471)B_z + (18.990)N$, where multiple determination coefficients R are 0.816.

Model	Unstandardized coefficients	Standardized coefficients		t	Sig.	95% confidence interval for B	
	B	Std. error	Beta			Lower bound	Upper bound
Constant	58.028	21.751		2.668	0.009	14.951	101.106
B_z (nT)	−33.471	3.510	−0.572	−9.536	0.000	−40.422	−26.520
N (1/cm^3)	18.990	3.026	0.377	6.275	0.000	12.997	24.984

Table 13: Regression coefficients and analysis of variance. Dst = $-(13.926) + (1.242)B_z$, where R is 0.381.

	Unstandardized Coefficients		Standardized Coefficients	t	Sig.
	B	Std. Err.	Beta		
B_z(nT)	1.242	0.277	0.381	4.476	0.000
Constant	−13.926	0.982		−14.179	0.000

	Sum of Squares	df	Mean Square	F	Sig.
Regression	2298.830	1	2298.830	20.031	0.000
Residual	13541.837	118	114.761		
Total	15840.667	119			

Table 14: Regression coefficients and analysis of variance. Dst = $-(10.803) + (0.696)B_z - (0.263)B_z^2$ where R is 0.481.

	Unstandardized Coefficients		Standardized Coefficients	t	Sig.
	B	Std. err.	Beta		
B_z(nT)	0.696	0.304	0.214	2.289	.024
B_z^2(nT)	−0.263	0.073	−0.338	−3.617	.000
Constant	−10.083	1.273		−8.487	.000

	Sum of Squares	df	Mean Square	F	Sig.
Regression	3660.911	2	1830.455	17.584	0.0000
Residual	12179.756	117	104.100		
Total	15840.667	119			

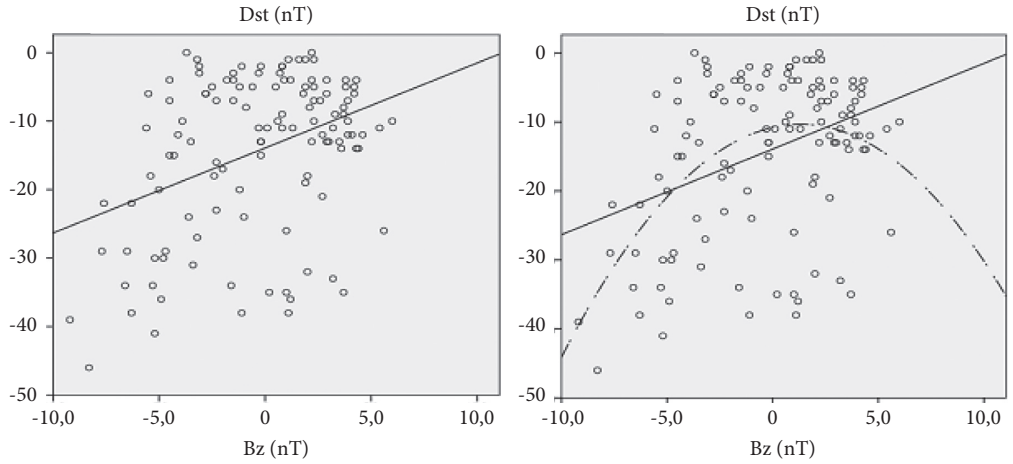

Figure 7: Linear and quadratic relation of Dst and B_z.

be seen in Tables 13 and 14 and Figure 7, the linear and quadratic relationships of the magnetic field component B_z with the Dst index.

In Tables 15 and 16 and Figure 8, the linear and quadratic relationships between the magnetic field component B_z and the ap index is presented.

In Tables 17 and 18 and Figure 9, the linear and nonlinear relationships between the magnetic field component B_z and the AE index is presented.

Ultimately, it would be appropriate to declare the proven [15, 16] model for this weak storm. This nonlinear model is a model that includes parameters P, N, and ap index. It is quite interesting that the model introduced by Eroglu for the first time demonstrates its consistency for a weak geomagnetic storm. The short reaction times of weak storms have been a difficult test for the stability of the model.

The nonlinear model is in the form $P = a + b \ln \mathrm{ap} + cN$, where a, b, and c are constants. The analysis of variance values of flow pressure (P) are shown in Table 19. The magnitudes of coefficients are $a = 0.101$, $b = 0.053$, and $c = 0.209$. Table 20 shows that all parameter estimation is in confidence interval of 95%. The model explaining this storm with 97% accuracy is:

Table 15: Regression coefficients and analysis of variance. ap = (7.360) − (1.263)B_z where R is 0.541.

	Unstandardized Coefficients		Standardized Coefficients	t	Sig.
	B	Std. Err.	Beta		
B_z(nT)	−1.263	0.181	−0.541	−6.986	0.000
Constant	7.360	0.640		11.502	0.000

	Sum of Squares	df	Mean Square	F	Sig.
Regression	2377.962	1	2377.962	48.809	0.000
Residual	5748.963	118	48.720		
Total	8126.925	119			

Table 16: Regression coefficients and analysis of variance. ap = (5.386) − (0.918)B_z + (0.167)B_z^2, where R is 0.600.

	Unstandardized Coefficients		Standardized Coefficients	t	Sig.
	B	Std. Err.	Beta		
B_z(nT)	−0.918	0.199	−0.393	−4.617	0.000
B^2_z(nT)	0.167	0.048	0.298	3.499	0.001
Constant	5.386	0.832		6.473	0.000

	Sum of Squares	df	Mean Square	F	Sig.
Regression	2922.661	2	1461.330	32.853	0.000
Residual	5204.264	117	44.181		
Total	8126.925	119			

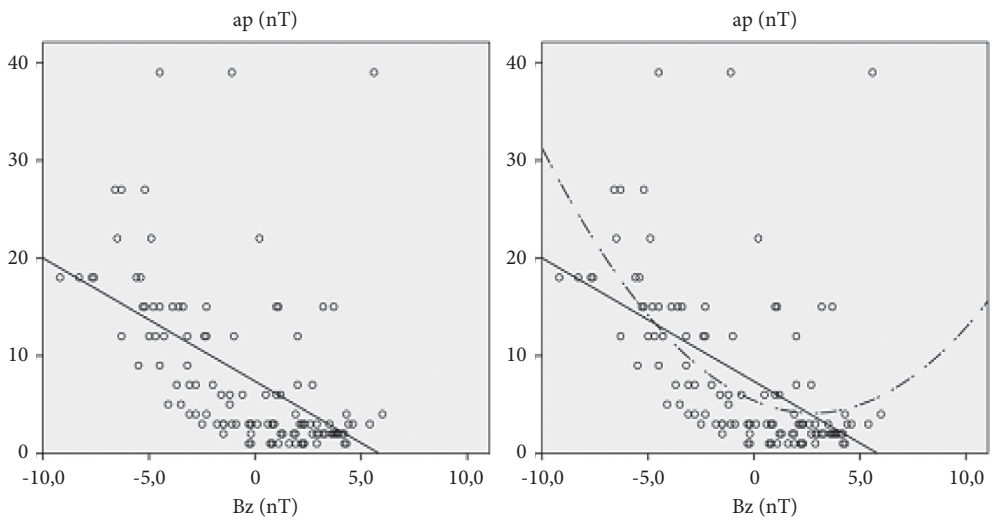

Figure 8: Linear and quadratic relation of ap and B_z.

Table 17: Regression coefficients and analysis of variance. AE = (175.595) − (43.544)B_z, where R is 0.745.

	Unstandardized Coefficients		Standardized Coefficients	t	Sig.
	B	Std. Err.	Beta		
B_z(nT)	−43.544	3.593	−0.745	−12.118	0.000
Constant	175.595	12.722		13.803	0.000

	Sum of Squares	df	Mean Square	F	Sig.
Regression	2827631.486	1	2827631.486	146.855	0.000
Residual	2272048.105	118	19254.645		
Total	5099679.592	119			

Table 18: Regression coefficients and analysis of variance. AE = (116.734) − (33.267)B_z + (4.965)B_z^2, where R is 0.806.

	Unstandardized Coefficients		Standardized Coefficients	t	Sig.
	B	Std. Err.	Beta		
B_z (nT)	−33.267	3.686	−0.569	−9.026	0.000
B_z^2 (nT)	4.965	0.882	0.355	5.627	0.000
Constant	116.734	15.423		7.569	0.000

	Sum of Squares	df	Mean Square	F	Sig.
Regression	3311582.290	2	1655791.145	108.343	0.000
Residual	1788097.302	117	15282.883		
Total	509969.592	119			

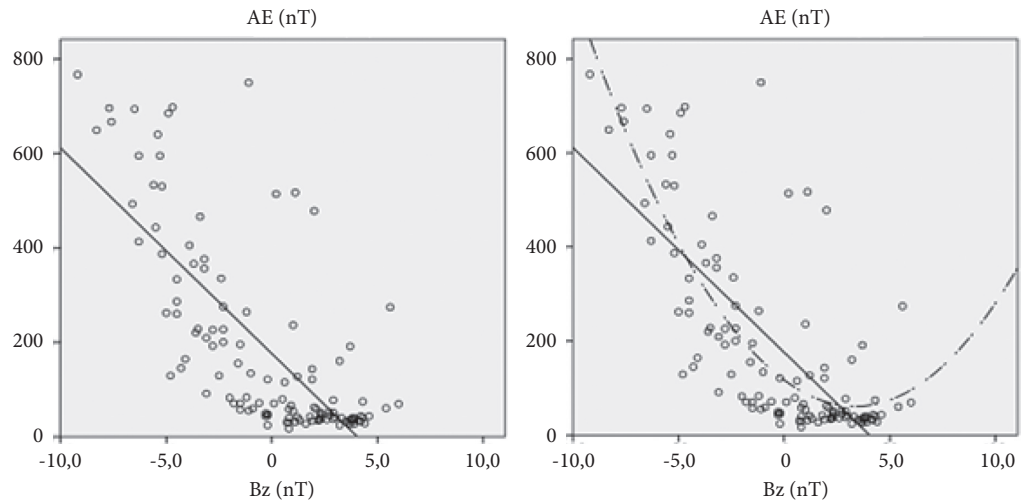

Figure 9: Linear and quadratic relation of AE and B_z.

Table 19: Anova (analysis of variance) of flow pressure P. P = (0.101) + (0.053)ln ap + (0.209)N.

Source	Sum of squares	df	Mean squares
Regression	370.748	3	123.853
Residual	2.996	117	0.026
Uncorrected total	373.744	120	
Corrected total	99.225	119	

Table 20: Parameter estimates. P = (0.101) + (0.053)ln ap + (0.209)N.

Parameter	Estimate	Std. error	95% confidence interval	
			Lower bound	Upper bound
a	0.101	0.028	0.045	0.157
b	0.053	0.022	0.009	0.097
c	0.209	0.005	0.198	0.220

4. Conclusion

The strength and consistency of the results obtained in moderate and strong geomagnetic events are also the goals of this weak geomagnetic storm study. Although the response time of the Dst (nT) index to the magnetic field is very short, it is noteworthy that the models are as efficient as in other kinds of storms. The 08 May 2014 geomagnetic storm is one of the weakest storms in the 24th solar cycle. I focus on the May 2014 weak storm. In the storm, solar wind parameters and zonal geomagnetic indices are discussed and the cause-effect relationship is obeyed. All possible binary or multiple relationship and model are presented to the reader even if not statistically significant. Every model that produced about the storm has been meticulously analyzed. In particular, the mathematical models involving solar wind pressure and proton density give an idea of the dynamic nature of the different plasmatic structures. In order for the model to be consistent, it is necessary to be validated by other storms. The last nonlinear model among flow pressure (P), ap, and proton density (N) explains the storm with 97% accuracy. All results are in the 95% confidence interval. Graphs and tables have visualized the correlation between zonal geomagnetic indices and solar wind parameters, as well as their interactions with each other.

Data Availability

The datasets used and/or analyzed during the current study are available from the corresponding author on reasonable request. The author utilizes the NASA CDA Web for OMNI Database (https://themis.igpp.ucla.edu/software.shtml) and Kyoto World Data Center for providing AE index and Dst index. She acknowledges the usage of ap and Kp index from the National Geophysical Data Center. The Dst index and AE data are provided by the World Data Center for Geomagnetism at Kyoto University. The data used in this article are available at the Data Center of NASA https://omniweb.gsfc.nasa.gov/form/dx1.html.

Conflicts of Interest

The author declares no conflicts of interest.

Authors' Contributions

Data are collected and analyzed by the author. All interpretations and explanations belong to the author. The author read and approved the final manuscript.

Acknowledgments

The author thanks the NASA, Kyoto University, and Kyoto World Data Center.

References

[1] S. I. Akasofu, "A source of the energy for geomagnetic storms and auroras," *Planetary and Space Science*, vol. 12, no. 801, 1964.

[2] R. K. Burton, R. L. Mcpherron, and C. T. Russell, "An empirical relationship between interplanetary conditions and Dst," *Journal of Geophysical Research*, vol. 80, no. 31, pp. 4204–4214, 1975.

[3] P. N. Mayaud, "Derivation, meaning, and use of geomagnetic indices," *Geophysical Monograph Series*, American Geophysical Union, Washington, DC, USA, 1980.

[4] T. Murayama, "Coupling function between solar wind parameters and geomagnetic indices," *Reviews of Geophysics*, vol. 20, no. 3, p. 623, 1982.

[5] G. Rostoker, E. Friedrich, and M. Dobbs, "Physics of magnetic storms," in *Magnetic Storms, Geophys. Monogr. Ser.*, B. T. Tsurutani, W. D. Gonzalez, Y. Kamide, and J. K. Arballo, Eds., vol. 98Washington, DC, USA, American Geophysical Union, 1997.

[6] B. T. Tsurutani, D. L. Judge, F. L. Guarnieri et al., "The October 28, 2003 extreme EUV solar flare and resultant extreme ionospheric effects: comparison to other Halloween events and the Bastille Day event," *Geophysical Research Letters*, vol. 32, no. 3, 2005.

[7] B. T. Tsurutani, O. P. Verkhoglyadova, A. J. Mannucci, G. S. Lakhina, G. Li, and G. P. Zank, "A brief review of "solar flare effects" on the ionosphere," *Radio Science*, vol. 44, no. 17, 2009.

[8] A. Hanslmeier, *The Sun and Space Weather. Astrophysics and Space Science*, Springer, Dordrecht, Netherlands, 2nd edition, 2007.

[9] G. S. Lakhina, S. Alex, B. T. Tsurutani, and W. D. Gonzalez, "Supermagnetic storms: hazard to society," *Extreme Events and Natural Hazards: The Complexity Perspective*, vol. 196, pp. 267–278, 2012.

[10] B. S. Rathore, D. C. Gupta, and K. K. Parashar, "Relation between solar wind parameter and geomagnetic storm condition during cycle-23," *International Journal of Geosciences*, vol. 5, no. 13, pp. 1602–1608, 2014.

[11] B. S. Rathore, D. C. Gupta, and K. K. Parashar, "Relation between solar wind parameter and geomagnetic storm condition during cycle-23," *International Journal of Geosciences*, vol. 5, no. 13, pp. 1602–1608, 2014.

[12] J. B. Habarulema, M. B. Dubazane, Z. T. Katamzi-Joseph, E. Yizengaw, M. B. Moldwin, and J. C. Uwamahoro, "Long-term estimation of diurnal vertical E × B drift velocities using C/NOFS and ground-based magnetometer observations," *Journal of Geophysical Research: Space Physics*, vol. 123, no. 8, pp. 6996–7010, 2018.

[13] D. Hampton, "A study of intense local dB/dt variations during two geomagnetic storms," *Space Weather*, vol. 16, p. 676, 2018.

[14] C. M. Ngwira, D. Sibeck, M. V. D. Silveira et al., "A study of intense local dB/dt variations during two geomagnetic storms," *Space Weather*, vol. 16, no. 6, pp. 676–693, 2018.

[15] E. Eroglu, "Mathematical modeling of the moderate storm on 28 February 2008," *New Astronomy*, vol. 60, pp. 33–41, 2018.

[16] E. Eroglu, "Modeling the superstorm in the 24th solar cycle," *Earth Planets and Space*, vol. 71, no. 1, pp. 1–12, 2019.

[17] E. Eroglu, "Modeling of 21 July 2017 geomagnetic storm," *Journal of Engineering Technology and Applied Sciences*, vol. 5, no. 1, pp. 33–49, 2020.

[18] E. Eroglu, "Zonal geomagnetic indices estimation of the two super geomagnetic activities of 2015 with the artificial neural networks," *Advances in Space Research*, vol. 68, no. 6, pp. 2272–2284, 2021.

[19] S. Chakraborty and S. K. Morley, "Probabilistic prediction of geomagnetic storms and the Kp index," *Journal of Space Weather and Space Climate*, vol. 10, no. 10, p. 36, 2020.

[20] K. Koklu, "Mathematical analysis of the 09 March 2012 intense storm," *Advances in Space Research*, vol. 66, no. 4, pp. 932–941, 2020.

[21] S. K. Sharma, A. K. Singh, S. K. Panda, and S. S. Ahemd, "The effect of geomagnetic storms on the total electron content over the low latitude Saudi Arab region: a focus on St. Patrick's day storm," *Astrophysics and Space Science*, vol. 365, no. 35, 2020.

[22] S. Inyurt, "Modeling and comparison of two geomagnetic storms," *Advances in Space Research*, vol. 65, no. 3, pp. 966–977, 2020.

[23] S. Bruinsma, C. Boniface, E. K. Sutton, and M. Fedrizzi, "Thermosphere modeling capabilities assessment: geomagnetic storms," *Journal of Space Weather and Space Climate*, vol. 11, no. 11, p. 12, 2021.

[24] E. Eroglu, *Dalga kilavuzlari boyunca geçici sinyallerin transferi*, Ph.D. dissertation, Gebze Institute of Technology, Gebze, Turkey, 2011.

[25] E. Eroglu, S. Aksoy, and O. A. Tretyakov, "Surplus of energy for time-domain waveguide modes," *Energy Education Science and Technology*, vol. 29, pp. 495–506, 2012.

[26] E. Eroglu, N. Ak, K. Koklu, Z. Ozdemir, N. Celik, and N. Eren, "Special functions in transferring of energy; a special case: "Airy function"" *Energy Education Science and Technology*, vol. 30, pp. 719–726, 2012.

[27] E. N. Parker, "Dynamics of the interplanetary gas and magnetic fields," *The Astrophysical Journal*, vol. 128, pp. 664–676, 1958.

[28] K. Shibata, S. Masuda, M. Shimojo et al., *The Astrophysical Journal Letters*, vol. 451, no. 2, pp. L83–L85, 1995.

[29] M. M. Fares Saba, W. D. Gonzalez, and A. L. Clúa de Gonzalez, "Relationships between the AE, ap and Dst indices near solar minimum (1974) and at solar maximum (1979)," *Annales Geophysicae*, vol. 15, no. 10, pp. 1265–1270, 1997.

[30] G. E. Brueckner, J.-P. Delaboudiniere, R. A. Howard et al., "Geomagnetic storms caused by coronal mass ejections (CMEs): march 1996 through June 1997," *Geophysical Research Letters*, vol. 25, no. 15, pp. 3019–3022, 1998.

[31] M. Temerin and X. Li, "Dstmodel for 1995–2002," *Journal of Geophysical Research*, vol. 111, no. A4, 2006.

[32] H. S. Fu, A. Vaivads, Y. V. Khotyaintsev et al., "Intermittent energy dissipation by turbulent reconnection," *Geophysical Research Letters*, vol. 44, no. 1, pp. 37–43, 2017.

[33] T. N. Davis and M. Sugiura, "Auroral electrojet activity index AE and its universal time variations," *Journal of Geophysical Research*, vol. 71, no. 3, pp. 785–801, 1966.

[34] J. Lin and T. G. Forbes, "Effects of reconnection on the coronal mass ejection process," *Journal of Geophysical Research: Space Physics*, vol. 105, no. A2, pp. 2375–2392, 2000.

[35] H. S. Fu, J. Tu, P. Song, J. B. Cao, B. W. Reinisch, and B. Yang, "The nightside-to-dayside evolution of the inner magnetosphere: imager for magnetopause-to-aurora global exploration radio plasma imager observations," *Journal of Geophysical Research: Space Physics*, vol. 115, no. A4, 2010.

[36] W. D. Gonzalez, B. T. Tsurutani, and A. L. Clúa de Gonzalez, "Interplanetary origin of geomagnetic storms," *Space Science Reviews*, vol. 88, no. 3-4, pp. 529–562, 1999.

[37] Y. Kamide, N. Yokoyama, W. Gonzalez et al., "Two-step development of geomagnetic storms," *Journal of Geophysical Research: Space Physics*, vol. 103, no. A4, pp. 6917–6921, 1998.

[38] M. Celebi, ZO. Ozdemir, E. Eroglu, and I. Guney, "Statistically defining optimal conditions of coagulation time of skim milk," *Journal of the Chemical Society of Pakistan*, vol. 36, no. 1, pp. 1–9, 2014.

[39] O. Isik, Z. F. Kocak, and E. Eroglu, "The investigation of surplus of energy and signal propagation at time-domain waveguide modes," *Applications and Applied Mathematics: International Journal*, vol. 9, no. 2, pp. 637–645, 2014.

[40] M. Sato and R. Kuwano, "Influence of location of subsurface structures on development of underground cavities induced by internal erosion," *Soils and Foundations*, vol. 55, no. 4, pp. 829–840, 2015.

[41] R. Tsay, "Analysis of financial time series," *Wiley Series in Probability and Statistics*, Wiley, New York, NY, USA, 2002.

[42] C. A. Loewe and G. W. Prölss, "Classification and mean behavior of magnetic storms," *Journal of Geophysical Research: Space Physics*, vol. 102, no. A7, Article ID 14209, 1997.

[43] M. Gilmore, C. X. Yu, T. L. Rhodes, and W. A. Peebles, "Investigation of rescaled range analysis, the Hurst exponent, and long-time correlations in plasma turbulence," *Physics of Plasmas*, vol. 9, no. 4, pp. 1312–1317, 2002.